Applied Catalysis B: Environment and Energy 348 (2024) 123797

Contents lists available at ScienceDirect

Applied Catalysis B: Environment and Energy

journal homepage: www.elsevier.com/locate/apcatb

Promoter or inhibitor: Self-tunable defense effects of $Ce(SO_4)_2$ against K and Zn co-poisoning over NO_x reduction catalysts

Lulu Wang, Jin Li, Tianwei Lan, Hailun Heyang, Huan Wang, Penglu Wang *, Dengsong Zhang *

International Joint Laboratory of Catalytic Chemistry, State Key Laboratory of Advanced Special Steel, Innovation Institute of Carbon Neutrality, Department of Chemistry, College of Sciences, Shanghai University, Shanghai 200444, China

ARTICLE INFO

Keywords:
NO_x reduction
Selective catalytic reduction
Heavy metal
Alkali metal
$Ce(SO_4)_2$

ABSTRACT

Selective catalytic reduction of NO_x with ammonia (NH_3-SCR) under the exposure of multiple poisons in fly ash remains a great challenging issue for environmental protection. Herein, the intelligently self-tunable defense effects of $Ce(SO_4)_2$ additive modification for the V_2O_5/CeO_2 catalyst with excellent resistance against K and Zn co-poisoning was originally illustrated. The $Ce(SO_4)_2$ additive could firstly act as an inhibitor to certainly restrain the electron transfer between V and Ce species to decrease the redox property, but the high NO_x reduction efficiency of $Ce(SO_4)_2$ modified fresh catalyst could be maintained due to the enhancement of vanadium species polymerization and acidity. Unexpectedly, the $Ce(SO_4)_2$ additive would smartly translate to act as a promoter over the co-poisoned catalyst to effectively combine with poisons, thus releasing most active vanadium species to exhibit superior co-poisoning resistance to K and Zn. This work provides a novel self-tunable multi-poisoning-resistant strategy via acid additive modification for SCR catalysts.

1. Introduction

Nitrogen oxides (NO_x), mainly including NO and NO_2, constitute a significant class of atmospheric pollutants responsible for environmental issues, such as haze, photochemical smog and acid rain [1–3]. The technique of selective catalytic reduction with NH_3 (NH_3-SCR) is considered as one of the most prominent and widely adopted methods to remove NO_x emitted from stationary sources [4–6]. However, the commercial V_2O_5/TiO_2 that is modified with WO_3 or MoO_3, still exhibits certain inherent drawbacks that are difficult to circumvent, including the biotoxicity of vanadium species and high SO_2 oxidation capacity during high-temperature stage [7,8]. In particular, under the circumstances of biomass-fired plants and solid waste incinerators, the existence of multiple poisons in the fly ash could lead to severe catalysts deactivation [9]. Thus, extensive efforts are dedicated to develop highly efficient NH_3-SCR catalysts with extraordinary resistance for multi-poisoning effects.

As the most prevalent poisons in the fly ash, alkali and heavy metals commonly coexist under practical conditions, which causes multi-poisoning effects on SCR catalysts. In recent years, considerable promoting strategies for multiplex metals concurrently poisoned catalysts have been discussed and investigated. An illustrative example, Li et al. observed that the existence of Ca and As weakened the interaction between As and CeO_2, thus restoring the reducibility and acid sites of the catalyst [8]. Moreover, Jing et al. found that the interaction between Ca and As facilitated the release of poisoned VO_x sites over VTi-Cd&As, which improved the SCR performance of VTi catalyst [10]. Recently, our research group designed a CeO_2-SnO_2 catalyst supported by SO_4^{2-}/TiO_2 superacid, enabling the migration of bulk SO_4^{2-} to the surface of catalysts, where the migrated SO_4^{2-} could bind with K and Pb, thereby achieving a self-protective effect for catalysts [11]. Additionally, we also unveiled that K and Cd can aggravate multiple poisoning on the $CeTiO_x$ catalyst, but the acid additive H-ZSM-5 can effectively capture K and Cd, leading to released Lewis acid sites and the subsequent restoration of SCR performance [12].

Nonetheless, rare attention concerning Zn-involved multi-poisoning-resistant SCR catalysts was paid in current studies, despite the stronger volatility and higher concentrations of Zn compared to Pb and Cd in fly ash of municipal solid waste incineration (MSWI) [13]. For SCR catalysts, the surface acidy and reducibility were severely reduced when 2 wt% ZnO was loaded, thus decreasing the SCR performance of catalysts [14]. Liu et al. reported that adding $Al_2(SO_4)_3$ to Mn/TiO_2 catalysts

* Corresponding authors.
E-mail addresses: plwang@shu.edu.cn (P. Wang), dszhang@shu.edu.cn (D. Zhang).

https://doi.org/10.1016/j.apcatb.2024.123797
Received 30 November 2023; Received in revised form 23 January 2024; Accepted 30 January 2024
Available online 2 February 2024

enhanced the resistance to Zn poisoning [15]. Furthermore, Jiang et al. found that Zn and As exhibited an offset effect on the VWTi catalyst, effectively reducing the poisoning impact of heavy metals on the catalyst [16]. However, the multi-poisoning-resistant strategies for the most prevalent alkali metal (K) and heavy metal (Zn) were scarcely reported, which exactly worth making more meaningful endeavors. Especially in biomass boilers and solid waste incinerators, the deactivation of SCR catalysts was attributed to high concentrations of K and Zn coexisting [17,18]. Due to its abundant acid sites and strong redox capacity, Ce$(SO_4)_2$ is usually employed for catalyst modification as catalytic additive, thereby enhancing redox properties and acidity of the catalyst [19]. Even so, there also remains a dearth of comprehensive investigations regarding the promoting and inhibitory effects of $Ce(SO_4)_2$ on SCR catalysts under multi-poisoning conditions, but it is significant to facilitate the regulation of chemical properties over catalysts and guide the rational design of multi-poisoning-resistant SCR catalysts.

Herein, the self-tunable defense mechanism of $Ce(SO_4)_2$ additive against K&Zn co-poisoning over CeO_2 supported V_2O_5 catalyst (V_2O_5/CeO_2) was proposed. The co-poisoning effects of K and Zn differ significantly depending on the tight interaction between poisons and the different sites among raw V_2O_5/CeO_2 catalyst or $Ce(SO_4)_2$ modified $V_2O_5/Ce(SO_4)_2$-CeO_2 catalyst. Combing different characterization methods, it has been proved that $Ce(SO_4)_2$ additive would first act as an inhibitor on the V_2O_5/CeO_2 catalyst to certainly decrease the redox property and impede the electron transfer between V and Ce species, but translate to a promoter to tightly combine with K and Zn poisons and release the active VO_x sites in K&Zn co-poisoned V_2O_5/CeO_2 catalysts, thus enhancing the multi-resistance against alkali and heavy metal poisons over SCR catalysts. This interesting discovery not only provides valuable insights into the mechanism of K and Zn co-poisoning over SCR catalysts, but also offers an effective approach for designing multi-poisoning-resistant catalysts in practical applications contains high amount of alkali and heavy metals.

2. Materials and methods

2.1. Catalysts preparation

The fresh V_2O_5/CeO_2 catalyst was synthesized by a typical impregnation method. The $V_2O_5/Ce(SO_4)_2$-CeO_2 catalyst was obtained using immersion method to physically mix $Ce(SO_4)_2$ (mass ratios of 10–50 wt % among modified catalysts) with CeO_2 support and then loaded with 3 wt% V_2O_5. Finally, the mixture was dried at 80 °C for 24 h and calcined at 450 °C for 4 h in static air with a ramping rate of 5 °C/min. For the $V_2O_5/Al_2(SO_4)_3$-CeO_2, $V_2O_5/Ce_2(SO_4)_3$-CeO_2 and $V_2O_5/Ti(SO_4)_2$-CeO_2 catalysts obtained via replacing $Ce(SO_4)_2$ by $Al_2(SO_4)_3$, $Ce_2(SO_4)_3$ and Ti$(SO_4)_2$, respectively, the same preparation was performed. The obtained samples were denoted as V/C, V/CSC, V/A_2S_3C, V/C_2S_3C and V/TSC, respectively.

K&Zn co-poisoning catalysts were obtained by impregnating potassium nitrate and zinc nitrate hexahydrate solution on fresh catalysts by loading 1 wt% K_2O and 2 wt% ZnO. The mixed solution was then transferred to an oven and dried under 80 °C for 24 h. Then the collected samples were finally calcined at 450 °C for 3 h in static air with a ramping rate of 5 °C/min. The co-poisoned samples were denoted as K&Zn-V/C, K&Zn-V/CSC, K&Zn-V/A_2S_3C, K&Zn-V/C_2S_3C and K&Zn-V/TSC, respectively.

2.2. NO_x reduction measurements

The 0.18 g catalyst with 20–40 meshes was assessed to measure the NO_x conversion in a fixed-bed quartz flow reactor (inner diameter = 7 mm). The composition of the gas mixture was: [NO] = 500 ppm, [NH_3] = 500 ppm, [O_2] = 5 vol%, and N_2 as balance. The total flow rate was set at 250 mL·min^{-1}, which was equivalent to a gas hourly space velocity (GHSV) of 100,000 h^{-1}. The gas concentrations of NO, NO_2, NH_3, H_2O, and N_2O were simultaneously monitored by an FTIR spectrometer (Thermo Fisher ANTARIS IGS Analyzer). The conversion of NO_x and the selectivity of N_2 were calculated to the following equation:

$$NO_x Conversion\left(\%\right) = \frac{[NO_x]_{in} - [NO_x]_{out}}{[NO_x]_{in}} \times 100\%$$

$$N_2 selectivity\left(\%\right) = \left(1 - \frac{2[N_2O]_{out}}{[NH_3]_{in} + [NO_x]_{in} - [NH_3]_{out} - [NO_x]_{out}}\right) \times 100\%$$

Where NO_x represents NO and NO_2. $[N_2O]_{out}$, $[NO_x]_{in}$, $[NO_x]_{out}$, $[NH_3]_{in}$, and $[NH_3]_{out}$ indicated the corresponding the inlet and outlet gas concentrations, respectively.

The elaborate catalysts preparation and measurements characterization were listed in the Supporting Information (SI).

3. Results and discussion

3.1. NO_x reduction evaluation

First, the effect of different acidic additives [$Ce(SO_4)_2$, $Al_2(SO_4)_3$ and $Ce_2(SO_4)_3$] on the resistance of alkali and heavy metals over the V/C catalyst was investigated (Figs. S1 and S2). It was revealed that $Ce(SO_4)_2$ emerged as the optimal acid additive with the highest resistance against alkali and heavy metals co-poisoning. Subsequently, a 10–50 wt% mass ratio of $Ce(SO_4)_2$ was utilized to combat K and Zn co-poisoning on the V/C catalyst (Figs. S3 and S4). As a result, the V/C catalyst modified with 30 wt% $Ce(SO_4)_2$ (V/CSC) exhibited the highest resistance to co-poisoning by K and Zn. Moreover, the NO_x conversion and N_2 selectivity of V/C, V/CSC, K&Zn-V/C and K&Zn-V/CSC catalysts in the temperature range of 150–420 °C was depicted in Fig. 1 A, under a gaseous hourly space velocity (GHSV) of 100,000 h^{-1}. Both V/C and V/CSC catalysts exhibited excellent SCR activity, demonstrating a broad operation window of 240–420 °C with the NO_x conversion above 80%. Meanwhile, the N_2 selectivity exceeded 90% within this operating window for both fresh catalysts. After co-poisoning by K and Zn, the NO_x conversion of contrast K&Zn-V/C and commercial K&Zn-VWT (Fig. S5) catalysts both stayed below 10%, displaying the severe deactivation of catalysts, and accompanying with the N_2 selectivity gradually decreased with the temperature increasing. In contrast, the K&Zn-V/CSC catalyst mostly retained its initial activity with over 80% of NO_x conversion from 240 to 420 °C, which indicated that the V/CSC catalyst revealed a better resistance to K and Zn co-poisoning.

With introducing 2% H_2O in Fig. 1B, the NO_x conversion of V/CSC was gradually higher than that of V/C as the temperature increased. Meanwhile, the V/CSC also exhibited higher K and Zn co-poisoning resistance than K&Zn-V/C. To evaluate the intrinsic reaction activity of catalysts, the reaction rate normalized with active V^{5+} contents (r_V^{5+}) that was obtained from X-ray photoelectron spectroscopy (XPS) was applied. It was indicated that the reaction rate of V/CSC was higher than that of V/C since 300 °C. After K and Zn co-poisoning, the reaction rate of K&Zn-V/CSC was also much higher than that of K&Zn-V/C. Significantly, the reaction rate of K&Zn-V/C was much lower than the fresh one in comparison to the little change in the reaction rate of V/CSC after co-poisoning. Thus, it was revealed that the V/CSC catalyst still exhibited superior resistance to K and Zn co-poisoning with the introduction of Ce$(SO_4)_2$ additive under humid conditions. Furthermore, the NO_x conversion of single K or Zn poisoned catalysts were also investigated on VWT, V/C and V/CSC (Figs. S5-S7). In the presence of K, the NO_x conversion of K-VWT and K-V/C showed a considerable decrease, while that of K-V/CSC slightly improved during 150–270 °C. Although the poisoning effect of Zn over catalysts was not such serious as that of K, the presence of Zn poison still caused serious deactivation on Zn-V/C and Zn-VWT, while the NO_x conversion of Zn-V/CSC only showed a slight decline. Furthermore, to explore the special characteristic of CeO_2 support, the $V_2O_5/Ce(SO_4)_2$-TiO_2 (V/CST) catalyst was obtained by replacing the CeO_2 support by TiO_2. Although V/CST exhibited similar

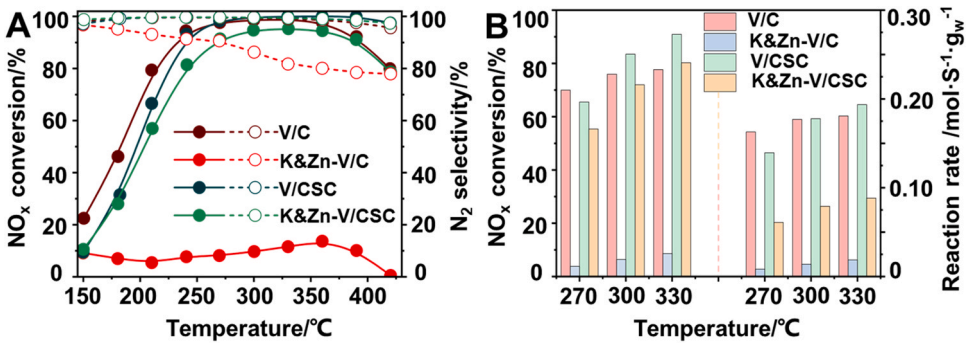

Fig. 1. (A) Plots of NO_x conversion (solid lines) and N_2 selectivity (dash lines) as a function of temperature over V/C, K&Zn-V/C, V/CSC and K&Zn-V/CSC catalysts. (B) Plots of NO_x conversion in 2% H_2O (when used) and the reaction rates normalized by V^{5+} contents (r_V^{5+}) over V/C, K&Zn-V/C, V/CSC and K&Zn-V/CSC catalysts from 270 ℃ to 330 ℃. Reaction conditions: 500 ppm of NH_3, 500 ppm of NO, 5 vol% O_2, 2% H_2O (when used) balanced with N_2, and 100,000 h^{-1} of GHSV. $r_V^{5+}=F_{NOx}*X_{NOx}/22.44*W_V^{5+}$, F_{NOx} was the concentration of inlet NO molecules (1.5 L/min), X_{NOx} was the NO_x conversion, and W_V^{5+} was the atomic ratio of V^{5+} in each catalyst.

NO_x reduction ability in comparison to V/CSC, the NO_x conversion obviously decreased over K&Zn-V/CST compared with K&Zn-V/CSC, which was ascribed to the special matching effects of CeO_2 support with $Ce(SO_4)_2$ acid additive (Figs. S8 and S9). Meanwhile, a similar phenomenon was observed over $V_2O_5/Ti(SO_4)_2$-CeO_2 (V/TSC) obtained via replacing $Ce(SO_4)_2$ by $Ti(SO_4)_2$ and $V_2O_5/Ti(SO_4)_2$-TiO_2 (V/TST) via replacing CeO_2 by TiO_2, which further verified the matching effects of CeO_2 with $Ce(SO_4)_2$. However, it was worth noting that the SCR performance of V/TSC was notably lower than that of V/CSC, which might be due to the abundant acid sites and strong redox capacity of $Ce(SO_4)_2$. In addition, although V/CSC and the catalyst with sulfation treatment (V/C-S) both exhibited excellent SCR activity, V/CSC expressed superior resistance to K and Zn co-poisoning than that with sulfation treatment (V/C-S), highlighting the advantage of the acid additive (Figs. S10 and S11). Moreover, when compared the NO_x reduction performance of Ce$(SO_4)_2$-CeO_2 (CSC), pure $Ce(SO_4)_2$ supported V_2O_5 (V/CS) and $Ce(SO_4)_2$-CeO_2 supported V_2O_5 (V/CSC), as well as their co-poisoned catalysts (K&Zn-CSC, K&Zn-V/CS and K&Zn-V/CSC), the superior activity and co-poisoning resistance of V/CSC catalyst emphasized the distinct characteristics and special matching effects of CeO_2 support with the active component V_2O_5 (Figs. S12 and S13). With the condition of NO_x conversion below 20% and GHSV higher than 200,000 h^{-1}, the apparent activation energy (E_a) of V/C, K&Zn-V/C (inactive), V/CSC and K&Zn-V/CSC catalysts were calculated according to the Arrhenius formula (Fig. S14). Specifically, the E_a values were determined as 24.72 kJ·mol^{-1} (V/C), 58.65 kJ·mol^{-1} (V/CSC) and 70.21 kJ·mol^{-1} (K&Zn-V/CSC), respectively. The results indicated that the reaction mechanism of V/CSC and K&Zn-V/CSC with acid additives modified was similar, but differed from that of V/C. It could be concluded that the $Ce(SO_4)_2$ additive modified CeO_2 supported V_2O_5 catalyst showed both excellent SCR activity and the resistance of alkali and heavy metals co-poisoning, which ensured the V/CSC catalyst to exhibit great application prospect among the NO_x reduction circumstance with high content of alkali and heavy metals.

3.2. Structure and reducibility analysis

To grasp the correlation between the co-poisoning resistance and the crystal structure of catalysts, X-ray power diffraction (XRD) was conducted. The characteristic peaks for all the catalysts in XRD pattern (Fig. S15) indicated that the main crystal phase was CeO_2 (PDF#81–0792). Furthermore, no peaks associated with V_2O_5 found was possibly the result of high dispersion of surface V_2O_5 species and taking shape amorphous species. The crystal structure of all the catalysts showed no significant variation before and after K and Zn co-poisoning. The thermogravimetry-differential scanning calorimetry (TG-DSC) was tested to explore the thermal stability of $Ce(SO_4)_2$ species over fresh and co-poisoned catalysts (Fig. S16). The $Ce(SO_4)_2$ species would be decomposed into $Ce_2(SO_4)_3$ species at about 500–600 ℃ [20], so that V/CSC and K&Zn-V/CSC calcined at 450 ℃ still could maintain more Ce$(SO_4)_2$ species. The total weight loss for V/CSC ((11.01%) and K&Zn-V/CSC (8.35%) was lower than that in V/C_2S_3C (12.59%) and K&Zn-V/C_2S_3C (10.25%) under N_2 flow, and a small number of SO_4^{2-} in $Ce_2(SO_4)_3$ was found to be decomposed into SO_2 over V/C_2S_3C during the SCR performance testing, indicating that $Ce(SO_4)_2$ was more stable than $Ce_2(SO_4)_3$ in catalysts and the total weight loss was decreased after co-poisoning compared with fresh catalysts. The presence of only one endothermic peak in fresh catalysts indicated that only one kind of sulfate species presented, while two endothermic peaks existed over co-poisoned catalysts validated the formation of other sulfate species such as K_2SO_4 and $ZnSO_4$. The content of S element (Table S1) quantitatively tested by inductively coupled plasma optical emission spectrometry (ICP-OES) exhibited that the S content among V/CSC (from 0.6 to 0.5) and V/50% CSC (from 0.8 to 0.7) before and after K and Zn co-poisoning were barely affected, which indicated that SO_4^{2-} species was relatively stable among catalysts even after co-poisoning. Furthermore, XPS and EDS results (Table S2) exhibited that S element was mostly present on the surface of V/CSC catalysts before and after co-poisoning, and K and Zn were also mostly deposited on the surface of K&Zn-V/C and K&Zn-V/CSC catalysts. Under this premise, it was possible for K and Zn were tended to bond with SO_4^{2-} species over K&Zn-V/CSC surface to improve the resistance to K and Zn co-poisoning. As a comparison, K and Zn preferred to bond with active VO_x species on the surface of K&Zn-V/C, thus causing the severe deactivation. According to the content of K (2.7 at%) and Zn (0.3 at%) on the K&Zn-V/CSC surface from XPS results, it was calculated that 2.85 at% S was required in theory to form K_2SO_4 and $ZnSO_4$, so that it could be preliminarily shown that the K and Zn could be completely bonded with SO_4^{2-} species (5.3 at% S on surface) introduced into the V/CSC catalyst. Scanning electron microscopy (SEM)-energy dispersion spectroscopy (EDS) mapping also revealed this conclusion, whether V/CSC was co-poisoned by K and Zn or not, V species and $Ce(SO_4)_2$ species were both well dispersed on the CeO_2 support (Figs. S17-S20). N_2 adsorption-desorption isotherm results (Fig. S21) showed that both fresh and K&Zn co-poisoned catalysts exhibited a comparable pore structure, manifesting that K and Zn co-poisoning expressed nearly no effect on the pore structure of catalysts. However, the pore volume and surface area both slightly decreased after K and Zn co-poisoning on the V/C catalyst, which was due to the successive coverage of alkali and heavy metals on the surface, thus leading to the inferior K and Zn co-resistance (Table S3). Interestingly, with the introduction of the $Ce(SO_4)_2$ acid additive, the specific surface area of the catalyst decreased obviously, which was probably owe to the agglomeration of the sulfate species. In addition, the increase in surface area of the K&Zn-V/CSC catalyst might be attributed to the change of

catalyst crystallinity caused by K and Zn co-poisoning.

To further investigate the intrinsic structure of all catalysts, Raman spectra were recorded. In Fig. 2 A, peaks at 715 cm^{-1}, 834 cm^{-1} and 915 cm^{-1} could be ascribed to V-O-V vibration mode, V-O-Ce species and polymeric vanadyl species, respectively, while the peak at 1000 cm^{-1} was assigned to the V═O species [21]. Moreover, peaks at 1053 cm^{-1} and 1171 cm^{-1} were corresponded to the monomeric vanadyl species and second-order longitudinal optical mode, respectively [21,22]. For the K&Zn-V/C catalyst, the V═O peak position shifted to lower wavenumbers, and the peak intensity of V═O and monomeric vanadyl species increased, which could be attributed to the introduction of K and Zn prolonged the bond length of V═O species and made active VO_x polymer translate to inactive monomers. Besides, the peak intensity of typical V-O-Ce characteristic was obviously weakened, indicating that K and Zn co-poisoning would restrain the interaction effect between V and Ce species, thus expressing adverse effects on the maintaining of high SCR performance. In contrast, the peak intensity of V-O-V was obviously weakened over V/CSC with the introduction of Ce$(SO_4)_2$ additive, stable and active polymeric vanadyl species generated and the peak intensity of V═O enhanced, which might be due to the fact that the V-O-V species were converted to active VO_x polymer or V═O species and also indicated that the vanadium species polymerization was enhanced with the utilization of Ce$(SO_4)_2$. Meanwhile, the peak of monomeric vanadyl species and V-O-Ce disappeared over V/CSC, which revealed that the Ce$(SO_4)_2$ additive might act as an inhibitor to markedly restrain the interaction effect of V and Ce species over the V/CSC catalyst. Moreover, the peak intensity of vanadyl species was weakened after co-poisoning, which manifested that alkali and heavy metals co-poisoning might affect the crystal shape of the catalyst, leading to decreased crystallinity and a more amorphous structure. More importantly, K and Zn poisons would prefer to combining with Ce$(SO_4)_2$ additive to undermine the effects of Ce$(SO_4)_2$ additive on the vanadium species polymerization due to the weakened intensity of polymeric vanadyl and V═O species.

Based on the edge energy (E_g) derived from ultraviolet visible (UV–vis) spectra was closely related to the extent of VO_x polymerization (Figs. S22-S24) [23], and the lower edge energy was corresponded to the higher polymerization of V species, the values of the band gap energy for V/CSC and V/C were calculated and estimated as 2.27 eV and 2.61 eV, respectively, which further verified the enhanced V species polymerization with the introduction of Ce$(SO_4)_2$ additive. After co-poisoning, lower E_g values of K&Zn-V/CSC (2.53 eV) was obtained compared with K&Zn-V/C (2.80 eV), suggesting that K and Zn made polymeric vanadyl species transfer into monomeric ones over K&Zn-V/C while the VO_x species of V/CSC were more stable. In short, Ce$(SO_4)_2$ acid additive could uniformly disperse on the CeO_2 support and obviously decrease the specific surface area of the catalyst, enhancing the polymerization of V species. After the co-poisoning of K and Zn, the active VO_x polymer would translate to inactive monomers and the effective V and Ce interaction would be suppressed over K&Zn-V/C. However, the enhanced polymerization of active V species caused by Ce$(SO_4)_2$ additive modification among V/CSC could be effectively maintained after K and Zn co-poisoning, which was resulted from the efficient combination of K and Zn poisons with Ce$(SO_4)_2$ additive over the K&Zn-V/CSC catalyst.

The redox properties of catalysts before and after K&Zn co-poisoning on V/C and V/CSC were assessed by temperature programmed reduction of H_2 (H_2-TPR) as shown in Fig. 2B, with the H_2 consumed by different species on each catalyst was calculated from the area of reduction peaks (Table S4). There were four reduction peaks in V/C, which could be explained to the reduction of V^{5+} to V^{3+} (385 ℃), the reduction of surface oxygen (surface Ce^{4+} to Ce^{3+} at 438 ℃), surface lattice oxygen of CeO_2 (469 ℃) and bulk Ce^{4+} to Ce^{3+} (730 ℃), respectively [24]. For the K&Zn-V/C, the reduction peaks moved toward lower temperature, which was due to K_2O and ZnO could act as certain electron promoter to boost the low-temperature redox property of catalyst to some extent. Besides, an additional reduction peak of metal oxides occurred over the K&Zn-V/C catalyst at 702 °C was owe to the reduction of K_2O and ZnO species that were originated from Ce-O-K and Ce-O-Zn structures generated by K and Zn tightly combing with CeO_2 sites, suggesting that there existed tight combination between K and Zn with CeO_2 to hinder the reduction of CeO_2 species. While the H_2 consumption of K&Zn-V/C (1.07 mmol/g) decreased compared to V/C (1.24 mmol/g), owing to the inert reduction of K_2O and ZnO over K&Zn-V/C. For V/CSC, there were only two peaks located at 562 ℃ and 569 ℃, which could be interpreted as the superimposed reduction of V^{5+} to V^{3+} and Ce^{3+} to Ce^{4+}, as well as the reduction of sulfate species, respectively. Compared with V/C, the reduction peaks of surface lattice oxygen of CeO_2 and bulk Ce^{4+} to Ce^{3+} disappeared and the reduction peaks of V/CSC shifted to a higher temperature, which manifested that Ce$(SO_4)_2$ additive impeded the electron transfer of V and Ce and reduced the redox properties of V/C. Similarly, S 2p XPS (Fig. S25) revealed the atomic ratio of S:Ce over CSC (0.513) and K&Zn-CSC (0.521) were both higher than those in V/CSC (0.437) and K&Zn-V/CSC (0.365), respectively, further demonstrating the presence of strong interaction between Ce$(SO_4)_2$ additive and active V species on the catalyst surface. Moreover, a reduction peak of surface

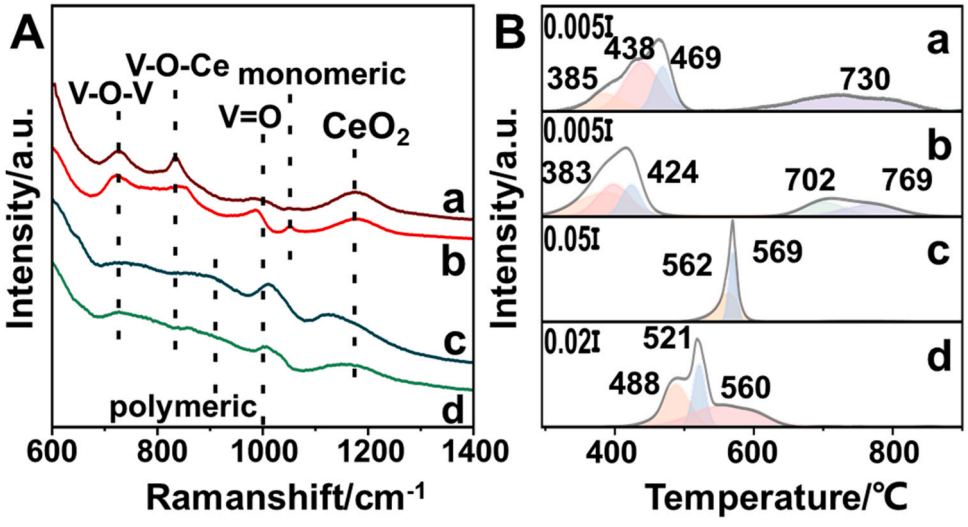

Fig. 2. (A) Raman spectra for fresh and co-poisoned catalysts. The inset is a partial enlargement of the above catalysts in Raman spectra from 600 to 1400 cm^{-1}. (B) H_2-TPR profiles of fresh and co-poisoned catalysts. Catalysts: (a) V/C, (b) K&Zn-V/C, (c) V/CSC and (d) K&Zn-V/CSC.

lattice oxygen assigned to CeO_2 species for K&Zn-V/CSC appeared at 560 °C, demonstrating that the inhibiting effects of $Ce(SO_4)_2$ additive was reduced to some extent on the electron transfer of V and Ce, which was resulted from the effective combination of $Ce(SO_4)_2$ additive with K and Zn poisons. There were no peaks of K_2O and ZnO species might be due to more stable sulfate species generated by K and Zn stably bonding with SO_4^{2-}. Beyond that, the increased H_2 consumption of K&Zn-V/CSC (4.68 mmol/g) compared to V/CSC (4.26 mmol/g) was due to the reduction of sulphate species accumulated on the surface of catalyst.

Furthermore, the activity of lattice oxygen species for catalysts were approximately estimated by O_2-TPD-MS (Fig. S26). The lattice oxygen species over K&Zn-V/C was more inactive than that of V/C due to the fact that the desorption of lattice oxygen moved to higher temperature (781 ℃) after K and Zn co-poisoning compared with V/C (740 ℃). However, due to the existence of $Ce(SO_4)_2$, the desorption temperature of K&Zn-V/CSC (726 ℃) was barely affected compared to V/CSC (748 ℃), which indicated that K and Zn were mainly bonded with Ce $(SO_4)_2$, thus still retaining most of active lattice oxygen over catalysts. All these results illustrated that the $Ce(SO_4)_2$ additive would act as an inhibitor to certainly restrain the electron transfer of V and Ce species among V/C catalyst, but translate to a promoter to effectively fix K and Zn poisons and released the active V sites among K and Zn co-poisoned catalysts, which successfully maintained the higher catalytic reactivity over K&Zn-V/CSC.

To further investigate the valence states and reducibility changes of elements among various catalysts, X-ray photoelectron spectroscopy (XPS) spectra of V 2p and Ce 3d were studied in Fig. 3 A, B. The peaks at 517.3 eV and 524.2 eV were assigned to the active V^{4+}, while peaks at 517.9 eV and 525.3 eV were assigned to the active V^{5+} [25]. As for K&Zn-V/C, the ratio of $V^{5+}/(V^{4+}+V^{5+})$ [$F(V^{5+})$ 30.7%] was slightly higher than that of V/C (28.7%), and the characteristic peak position of V $2p_{3/2}$ moved to the lower binding energy, which was attributed to the fact that K and Zn mainly bonded with V═O or V-O-V on the surface of K&Zn-V/C to affect the chemical state of active V^{5+} species. The initial F (V^{5+}) ratio on V/CSC (31.4%) did not significantly change compared with V/C, indicating that the introduction of $Ce(SO_4)_2$ additive only modulated the structure of VO_x species. For K&Zn-V/CSC, the $F(V^{5+})$ ratio (60.8%) increased significantly compared with V/CSC, which might be due to the fact that SO_4^{2-} was in excess caused by less SO_4^{2-} groups needed to form K_2SO_4 and $ZnSO_4$ compared to the intrinsic chemical constitute of $Ce(SO_4)_2$ in K&Zn-V/CSC, thus some V^{n+} deposited on the catalyst surface preferred to exist in the form of V^{5+} to balance the negative charge of superfluous SO_4^{2-} in the catalyst skeleton. Moreover, the changeable status of the V valence over K&Zn-V/CSC further hinted that the combination of K and Zn poisons with $Ce(SO_4)_2$ additive rather than active V species, thus restoring the high SCR activity of V/CSC after co-poisoning.

Moreover, Ce 3d XPS was also analyzed and presented in Fig. 3B. The raw Ce 3d spectra of fresh and K&Zn co-poisoned V/C and V/CSC catalysts were split into eight overlapping peaks. The peaks marked v and u represented the surface Ce^{3+} with the $3d^{10}$ 4 f^1 electronic state, whereas other peaks marked v^0, v′, v", u^0, u′ and u" represented the surface Ce^{4+} with $3d^{10}$ 4 f^0 state. Normally, the content of Ce^{3+} was crucial for SCR reactions, as it is often associated with oxygen vacancies that facilitate the redox cycle [26,27]. Therefore, according to the deconvoluted Ce 3d XPS spectra, the surface $Ce^{3+}/(Ce^{3+}+Ce^{4+})$ [$F(Ce^{3+})$] ratios of V/C and V/CSC before and after co-poisoning were calculated. After K and Zn co-poisoning over V/C, the content of $F(Ce^{3+})$ increased slightly (from 15.7% to 16.2%), and the characteristic peak position of Ce moved to the lower binding energy, which could be related to the introduction of K and Zn mainly bonded with Ce-O-V on the surface of K&Zn-V/C to affect the chemical state of active V^{4+} sites and also brought the increase of Ce^{3+} species. Owe to the introduction of $Ce(SO_4)_2$ additive, the original state of the V/CSC catalyst was disrupted and the redox cycle of $Ce^{3+} + V^{5+} \leftrightarrow Ce^{4+} + V^{4+}$ was inhibited, thus the $F(Ce^{3+})$ ratio of V/CSC (21.0%) was clearly higher than that of V/C. After K and Zn co-poisoning, the dramatically increased $F(V^{5+})$ ratio would promote the redox cycle of $Ce^{3+} + V^{5+} \leftrightarrow Ce^{4+} + V^{4+}$, thus causing a certain decrease in the $F(Ce^{3+})$ ratio of K&Zn-V/CSC (17.9%), which was consistent with the H_2-TPR result. Furthermore, the higher Zn 2p binding energy of K&Zn-V/CSC than that of K&Zn-V/C was mainly due to the fact that the electronegativity difference between Zn (1.6) and S (2.5) element over K&Zn-V/CSC was higher than that of between Zn and V (1.6) as well as Ce (1.12) elements over K&Zn-V/C, which caused more electrons lost around Zn atoms over K&Zn-V/CSC (Fig. S27). In addition, the O 1 s spectra exhibited two main characteristic peaks at 529.9 and 531.2 eV, representing lattice oxygen (O_β) and chemisorbed oxygen (O_α) species, respectively (Fig. S28) [24]. O_α is known to migrate more easily than O_β in oxidation reactions, contributing to the smooth redox cycle [28]. The $O_\alpha/(O_\alpha + O_\beta)$ [$F(O_\alpha)$] ratios among V/C and K&Zn-V/C were both 35.2%, which was likely owe to the superimposed effects of the decreased active oxygen species from the affected V sites and the increased surface oxygen species from the covered of K_2O and ZnO substances on the surface of K&Zn-V/C. The higher amount of O_α among V/CSC (54.1%) compared with V/C was mainly due to the contribution of SO_4^{2-} in $Ce(SO_4)_2$. However, the lower content of O_α among K&Zn-V/CSC (43.9%) than that of V/CSC was due to the addition of K and Zn after co-poisoning.

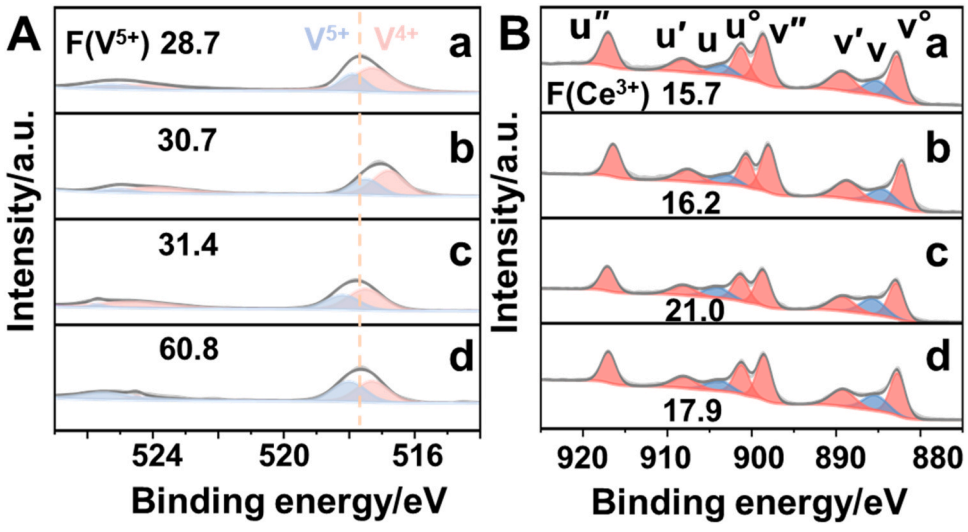

Fig. 3. (A) V 2p XPS spectra, and (B) Ce 3d XPS spectra for fresh and co-poisoned catalysts. Catalysts: (a) V/C, (b) K&Zn-V/C, (c) V/CSC and (d) K&Zn-V/CSC.

Density functional theory calculations were implemented to further expound the role of $Ce(SO_4)_2$ in enhancing the resistance of K and Zn co-poisoning over the V/C catalyst, with the computational models and most stable configuration with different poisons deposited were shown in Fig. 4. According to the XRD results, the main exposed facet of CeO_2 support among all catalysts was [111] plane, thus the computational model of V/C-[111] was established by placing a V_2O_5 group on the surface of CeO_2-[111] crystal plane. While the model of CSC-[111] was established by placing a S_2O_8 group on the surface of CeO_2-[111], then a V_2O_5 group placed on the surface of CSC-[111] was established to represent the computational model of V/CSC-[111] (Fig. S29). Moreover, the K_2O and ZnO groups set on the surface of CeO_2-[111], V/C-[V-O], V/CSC-[V-O] and V/CSC-[S-O] were established to investigate the adsorption energy of K and Zn poisons on different binding sites including S-O sites among V/CSC as well as V-O sites among V/C and V/CSC catalysts. As a result, the most stable adsorption energy of K_2O on V/C-[111] (−3.68 eV) was higher than that on CeO_2-[111] (−2.98 eV), meanwhile, the adsorption energy of ZnO on V/C-[111] (−0.25 eV) was found to almost the same as that on CeO_2-[111] (−0.31 eV), indicating that K_2O apt to bind to VO_x sites while ZnO not only tended to combine with VO_x sites but also on CeO_2 sites. After $Ce(SO_4)_2$ additive was introduced, the adsorption energy of K_2O on V/CSC-[V-O] (−5.43 eV) was lower than that on V/CSC-[S-O] (−4.89 eV), which indicated that K_2O was preferred to be fixed on the $Ce(SO_4)_2$ sites rather than VO_x sites. Furthermore, the adsorption energy of ZnO on V/CSC-[S-O] (−3.53 eV) was also lower than that on V/CSC-[V-O] (−3.07 eV), indicating that the VO_x sites could be expectedly released due to the stronger interaction between ZnO and $Ce(SO_4)_2$ sites, ensuring the V═O active sites can still be well maintained over K&Zn-V/CSC to participate in SCR reaction. In addition, caused by the results of ZnO not only bonded with SO_4^{2-} sites, but also fixed on Ce-O sites, the NO_x conversion of Zn-V/CSC was relatively decreased compared with that of K-V/CSC. Thereby, these computational results proved that K_2O and ZnO both bonded with active VO_x sites over V/C-[111], causing the serious deactivation of V/C catalyst. While due to the bonding effect between $Ce(SO_4)_2$ with K_2O and ZnO were more stable than that of between VO_x with K_2O and ZnO, the active VO_x sites were released and the resistance of K and Zn co-poisoning was enhanced over the V/CSC catalyst, which was consistent with the Raman and H_2-TPR. Compared with previous reports [11,12,29], the $Ce(SO_4)_2$ additive could not only act as an inhibitor to certainly restrain the electron transfer between V and Ce species to decrease the redox property but also could as a promoter over the co-poisoned catalyst to effectively combine with poisons, thus proposing a new self-tunable multi-poisoning-resistant strategy via acid additive modification for SCR catalysts.

3.3. Acidity and adsorption behavior study

To investigate the acidic properties of V/C and V/CSC catalysts before and after co-poisoning, ammonia temperature-programmed desorption-mass spectrometry (NH_3-TPD-MS) was carried out in Fig. 5 A. According to the MS signals of NH_3 desorption were split into five peaks over catalysts, the calculated NH_3 desorption amount by each desorption peak area was listed (Fig. S30 and Table S5). For the V/C catalyst, the NH_3 desorption peaks at 160 ℃ and 189 ℃ (weak acid sites), 228 ℃ and 289 ℃ (medium-strong acid sites), and 365 ℃ (strong acid sites) were observed. After co-poisoning, these reduction peaks moved to a lower temperature, as well as the amount of NH_3 adsorption also decreased from 0.78 μmol/g to 0.24 μmol/g, suggesting that K and Zn would interact with V species in the catalyst and result in the decline of the thermal stability and amount of adsorbed NH_3 species. Generally, four NH_3 molecules can be adsorbed by one V═O species and the adsorption capacity of $Ce(SO_4)_2$ to NH_3 was relatively weaker than that of V═O species [30], thus the acid amount of V/CSC was obviously lower than that of V/C. While a reverse phenomenon was observed before and after K and Zn co-poisoning over V/CSC, that is all the desorption peaks moved to higher temperature, with the amount of total acid sites significantly increased from 0.41 μmol/g to 0.96 μmol/g. The increasing amount of weak and medium strong acid sites was attributed to the exposure of VO_x sites due to the tightly combination of SO_4^{2-} sites by K and Zn, thus adsorbing more NH_3 species. While the increasing amount of strong acid sites was due to the fact that the NH_3 adsorption capacity of $ZnSO_4$ (3.2 μmol/g) was significantly higher than that of K_2SO_4 (0 μmol/g) and $Ce(SO_4)_2$ (0.29 μmol/g), thus the newly formed $ZnSO_4$ substances would provide more stable acid sites among K&Zn-V/CSC (Fig. S31 and Table S6). However, it should be noted that the increasement of strong acidity cannot be regarded as a unilaterally promoted factor to reveal the different SCR performances over co-poisoned catalysts, owing to the relatively inert properties of $ZnSO_4$.

Pyridine-IR was further conducted to clarify the type of acid sites located on catalysts (Fig. S32). As shown in Fig. 5B, the pyridine-IR spectra showed the results of pyridine adsorption on catalysts for 10 min at 30 °C. In the case of V/C, the absorption peaks around 1441 cm^{-1} and 1601 cm^{-1} were ascribed to Lewis acid sites [31,32], while the absorption peaks near 1540 cm^{-1} and 1575 cm^{-1} were corresponded to Brønsted acid sites [29,33]. Additionally, the absorption peak near 1481 cm^{-1} belonged to the sum of Lewis and Brønsted acid sites [34]. With the introduction of $Ce(SO_4)_2$ additive, the amount of Brønsted acid on V/CSC observably increased, which was resulted from the fact that the SO_4^{2-} group in the existence of water would provide certain hydroxy species that own Brønsted acidity [35]. After co-poisoning, the amount of Brønsted acid and Lewis acid among K&Zn-V/C were clearly decreased compared with V/C, which was mainly due to the occupation of K and Zn poisons on V sites that can both provided Brønsted acidity (V-OH) and Lewis acidity (V═O). However, although K and Zn co-poisoning significantly decreased the amount of Brønsted acid, the Lewis acid intensity of K&Zn-V/CSC was distinctly increased in contrast with the fresh catalyst. As the presence of $Ce(SO_4)_2$ provided more Brønsted acids and active V sites were well protected among K&Zn-V/CSC, the declined Brønsted acidity can still be

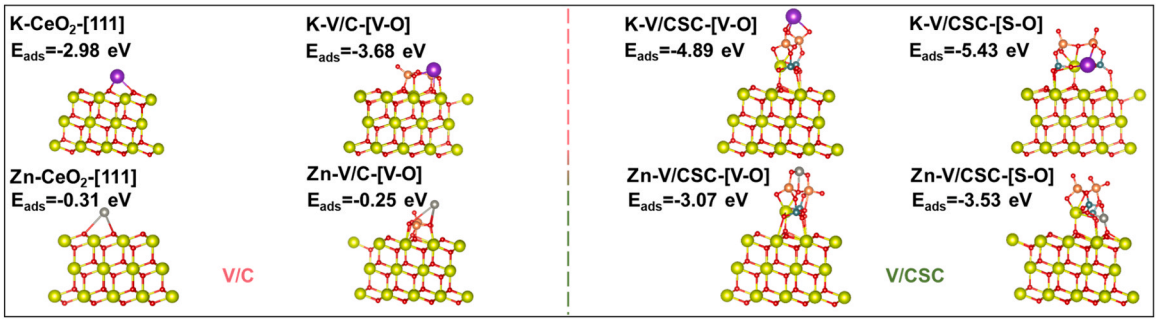

Fig. 4. DFT calculation models and the adsorption energies (E_{ads}) of the K_2O and ZnO unit on the most stable structures for CeO_2, V/C-[V-O], V/CSC-[V-O] and V/CSC-[S-O].

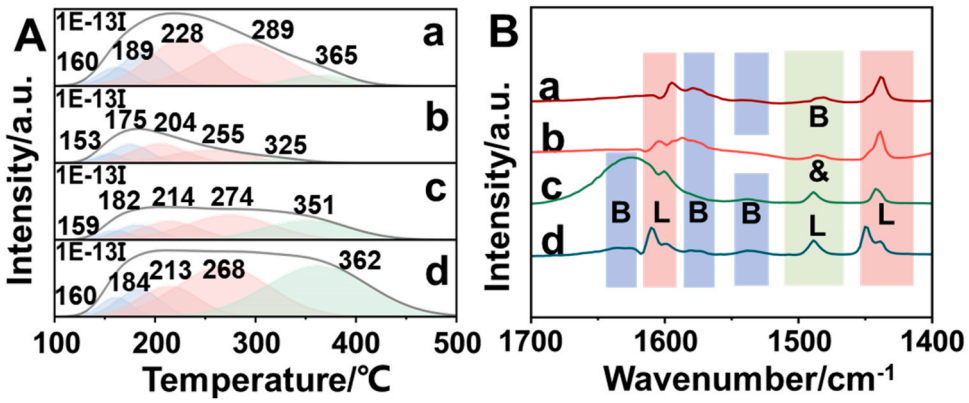

Fig. 5. (A) NH_3-TPD-MS profiles, and (B) Pyridine-IR spectra for fresh and co-poisoned catalysts. Catalysts: (a) V/C, (b) K&Zn-V/C, (c) V/CSC and (d) K&Zn-V/CSC.

attributed to the effective combination of K and Zn poisons with Ce $(SO_4)_2$ and the increase of Lewis acidity was due to the well maintained V═O sites. Furthermore, as shown in Fig. 6, the charge difference distribution results were obtained based on the DFT calculation in Fig. 4 to further study the electron gain and loss status among fresh and co-poisoned catalysts. It was revealed that V atom lost 0.028 |e| and 0.007 |e| electrons and transferred to O atom nearby among K-V/C-[V-O] and Zn-V/C-[V-O], respectively. Meanwhile, the phenomenon of the cyan area near the V atom showed a loss of electrons was well corresponded to an increase in the content of V^{5+} after K and Zn co-poisoning in the V 2p XPS results. In contrast, for K-V/CSC-[S-O] and Zn-V/CSC-[S-O], it can be clearly seen that K and Zn lost electrons while the yellow area near the V atom demonstrated a gain of 0.013 |e| and 0.002 |e| electrons, respectively, which reduced the valence state of V species and increased the amount of Lewis acid in K&Zn-V/CSC, well in keeping with the pyridine-IR results.

To further elucidate the NH_3 adsorption capacity of catalysts, the adsorption of NH_3 on the catalysts was tested by in situ NH_3 breakthrough at 240 ℃. As shown in Fig. 7A and Table S7, the adsorbed NH_3 amount over V/C (254 μmol/g) was higher than that over V/CSC (233 μmol/g), which was caused by the higher NH_3 adsorption capacity of V-OH and V═O sites than $Ce(SO_4)_2$ species. After the co-poisoning of K and Zn over V/C, the amount of adsorbed NH_3 was reduced by 30 μmol/g due to the poisoning effect of poisons over acid sites. While the amount of adsorbed NH_3 over K&Zn-V/CSC was increased by 26 μmol/g due to the generation of $ZnSO_4$ and exposure of acid sites, which was already proved in NH_3-TPD-MS. In addition, the adsorption behavior of NO on catalysts was researched by in situ NO breakthrough at 240 ℃. As shown in Fig. 7B and Table S7, the NO adsorbed amount over K&Zn-V/C (56 μmol/g) was higher than that in V/C (42 μmol/g), which could be explained by the formation of K_2O and ZnO over V/C promoted the adsorption of NO. However, the amount of adsorbed NO over V/CSC (37 μmol/g) was closed with that in K&Zn-V/CSC (35 μmol/g), which might be owe to the protective effects of $Ce(SO_4)_2$ additive, thus the active species of K&Zn-V/CSC were stable and the process of adsorbed NO was barely impacted.

To research the thermostability and the desorption behaviors of adsorbed NH_3 species, in situ diffuse reflectance infrared Fourier transform spectroscopy (in situ DRIFTS) NH_3 desorption was characterized (Fig. S33). As shown in Fig. 8A, the desorption of NH_3 species from in situ DRIFTS was exhibited at 100 °C, with the peaks of 1044 cm^{-1}, 1085 cm^{-1}, 1131 cm^{-1} and 1569 cm^{-1} were attributed to adsorbed NH_3 species bond to Lewis acid sites, while the peaks of 1434 cm^{-1}, 1457 cm^{-1} and 1649 cm^{-1} were ascribed to NH_4^+ species adsorbed on Brønsted acid sites over catalysts [36–42]. Compared to the V/C catalyst, the number of NH_3 species and NH_4^+ species were obviously increased among K&Zn-V/C, which was likely due to the increase in the content of V_2O_5 crystallites after co-poisoning. Besides, the intensity of Brønsted acid sites of V/CSC was significantly higher compared with V/C, which was ascribed to the stronger adsorption of NH_3 species by SO_4^{2-} groups on the catalyst surface. After co-poisoning, the amount of Brønsted acid sites showed a decrease due to the consumption of SO_4^{2-} by K and Zn on the surface of V/CSC, but still maintained more Brønsted acid sites in K&Zn-V/CSC. To compare the adsorption rate of NH_3 species over catalysts before and after K and Zn co-poisoning, in situ DRIFTS of NH_3 adsorption along adsorption time was performed (Fig. S33). The adsorption of NH_3 for 10 min under 240 ℃ was applied and the bond at 1687 cm^{-1} ascribed to NH_4^+ on the Brønsted acid sites was chosen to deeply illustrate the NH_3 adsorption rates (Fig S34). After K and Zn co-poisoning, despite the formation of NH_4^+ species over K&Zn-V/C and K&Zn-V/CSC both slowed down, but only the accumulation rate of NH_4^+ species over K&Zn-V/C was badly inhibited while that over K&Zn-V/CSC still satisfied the NO_x catalytic reduction due to the special protective effect of $Ce(SO_4)_2$.

In situ DRIFTS of NO + O_2 desorption was tested to further determine the type of adsorbed NO_x species at 100 °C in Fig. 8B, accompanying with the variation of adsorbed NO_x species along temperature raised were also recorded (Fig. S35). There were three types of NO_x species adsorbed on V/C and K&Zn-V/C, including monodentate nitrates (1040 cm^{-1}, 1091 cm^{-1}, 1311 cm^{-1} and 1515 cm^{-1}) [43–45], *cis*-N_2O_2

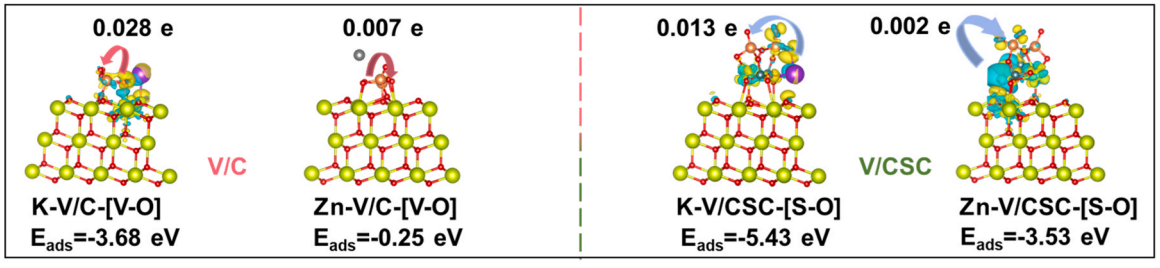

Fig. 6. The charge difference distribution of the K_2O and ZnO unit on the most stable structures of V/C-[V-O] and V/CSC-[S-O] from different visual angles with the isosurface at 0.00166392 e/$Bohr^3$. The yellow (cyan) isosurface represents the increase (decrease) of charge density.

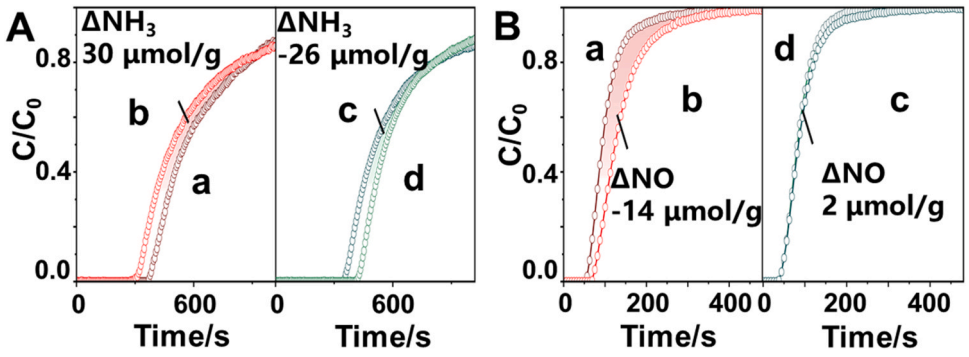

Fig. 7. *In situ* (A) NH_3 (1 vol% NH_3/He), and (B) NO+O_2/He (0.2 vol% NO+O_2/He) adsorption breakthrough curves of fresh and co-poisoned catalysts. Catalysts: (a) V/C, (b) K&Zn-V/C, (c) V/CSC and (d) K&Zn-V/CSC.

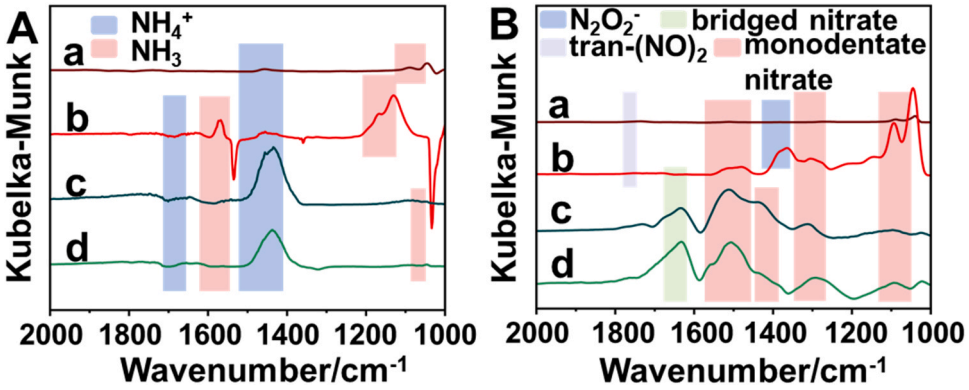

Fig. 8. *In situ* DRIFTS of (A) NH_3 (1000 ppm), and (B) NO (1000 ppm) + O_2 (5 vol% O_2/He) desorption results at 100 °C for fresh and co-poisoned catalysts. Catalysts: (a) V/C, (b) K&Zn-V/C, (c) V/CSC and (d) K&Zn-V/CSC.

(1372 cm^{-1}) [46], NO_2 (1622 cm^{-1}) [47] and trans-$(NO)_2$ (1742 cm^{-1}) [48]. After co-poisoning, the higher intensity of adsorbed NO_x species of K&Zn-V/C was due to the formation of K_2O and ZnO induced to generate more inactive and thermally stable NO_x species. In contrast, there were two kinds of adsorbed NO_x species over V/CSC and K&Zn-V/CSC, such as monodentate nitrates (1097 cm^{-1}, 1315 cm^{-1}, 1434 cm^{-1} and 1515 cm^{-1}) [43,44] and bridged nitrates (1632 cm^{-1}) [48]. The intensity of adsorbed NO_x species were barely impacted before and after K and Zn co-poisoning, which was due to the protection of $Ce(SO_4)_2$ over the K&Zn-V/CSC catalyst. Moreover, the adsorbed NO_x species were easily desorbed on the K&Zn-V/CSC surface, which could participate in the NH_3-SCR reaction more easily (Fig. S30). In a word, $Ce(SO_4)_2$ not only could induce to form more new adsorbed sites on the catalyst surface to increase the adsorption capacity of V/C catalyst to NH_3, but also could protect the active VO_x sites and the adsorption process of NH_3/NO species to complete the SCR reaction smoothly from the damage of K and Zn.

3.4. Transient reaction mechanism investigation

To investigate the variation of adsorbed species, active intermediate species and SCR reaction paths before and after K and Zn co-poisoning on V/C and V/CSC catalysts, in situ DRIFTS of the transient reactions for catalysts was executed at 240 ℃. In terms of the transient reactions between NO + O_2 and the pre-adsorption of NH_3 (Fig. S36), the reaction between the pre-adsorption of NH_3 on Lewis acid sites and NH_4^+ on the Brønsted acid sites with NO + O_2 was swimmingly carried out over V/C and V/CSC. Afterwards, due to the V_2O_5 sites were impaired by K and Zn co-poisoning, the adsorption of NH_3 was markedly weakened and the inert nitrates were accumulated on K&Zn-V/C. While the intensity of adsorbed NH_3 species was increased over K&Zn-V/CSC, which was due to the recovery of active V sites and the formation of $ZnSO_4$. After the introduction of NO + O_2, a few active nitrates were generated as the reaction progressed and an equilibrium between the consumption of NH_3 species and the adsorption of NO_x on the K&Zn-V/CSC surface was established. As shown in Fig. 9, in situ DRIFTS of transient reactions between NH_3 and pre-adsorbed NO_2 + O_2 was also performed at 240 °C. For V/C, adsorption peaks at 1036 cm^{-1}, 1292 cm^{-1}, 1363 cm^{-1} and 1540 cm^{-1} were all attributed to monodentate nitrates [45,48,49]. Upon the introduction of gaseous NH_3, all adsorbed NO_x species slowly disappeared, and corresponding NH_3 on Lewis acid sites (1157 cm^{-1}, 1305 cm^{-1} and 1556 cm^{-1}) and NH_4^+ on Brønsted acid sites (1465 cm^{-1} and 1671 cm^{-1}) emerged [36,50,51]. After the pretreatment with NO + O_2 for K&Zn-V/C, the monodentate nitrates (1010 cm^{-1}, 1204 cm^{-1}, 1293 cm^{-1}, 1358 cm^{-1} and 1503 cm^{-1}) and bidentate nitrate (1578 cm^{-1}) were generated [52–54]. Whereas, with the introduction of NH_3, stable monodentate nitrates were slightly consumed, and the adsorption of NH_3 (1030 cm^{-1} and 1219 cm^{-1}) were seriously inhibited [39], indicating that co-poisoning of K and Zn not just decreased the catalytic reactivity between adsorbed NH_3 species and NO_x species, but also resulted in the decline of surface acidity of the K&Zn-V/C catalyst.

In the matter of V/CSC, when NH_3 was introduced into the reaction, the adsorption of monodentate nitrates (1370 cm^{-1}, 1503 cm^{-1} and 1606 cm^{-1}) disappeared [47,55,56], accompanying with adsorbed NH_3 (1308 cm^{-1} and 1569 cm^{-1}) [54] and NH_4^+ (1424 cm^{-1} and 1677 cm^{-1}) [56] species occurred. The reaction rate of nitrates species over V/CSC was faster than that of V/C. For K&Zn-V/CSC, upon the introduction of NH_3, despite the presence of stable trans-$(NO)_2$ (1786 cm^{-1}) [41], monodentate nitrates (1339 cm^{-1}, 1458 cm^{-1} and 1542 cm^{-1}) [57,58] and N_2O_4 (1694 cm^{-1}) [44] gradually disappeared. Additionally, the adsorption of NH_3 (1522 cm^{-1} and 1554 cm^{-1}) [36,56] and NH_4^+ (1436 cm^{-1}, 1660 cm^{-1}, 1718 cm^{-1}, and 1774 cm^{-1}) [38,45,53] were

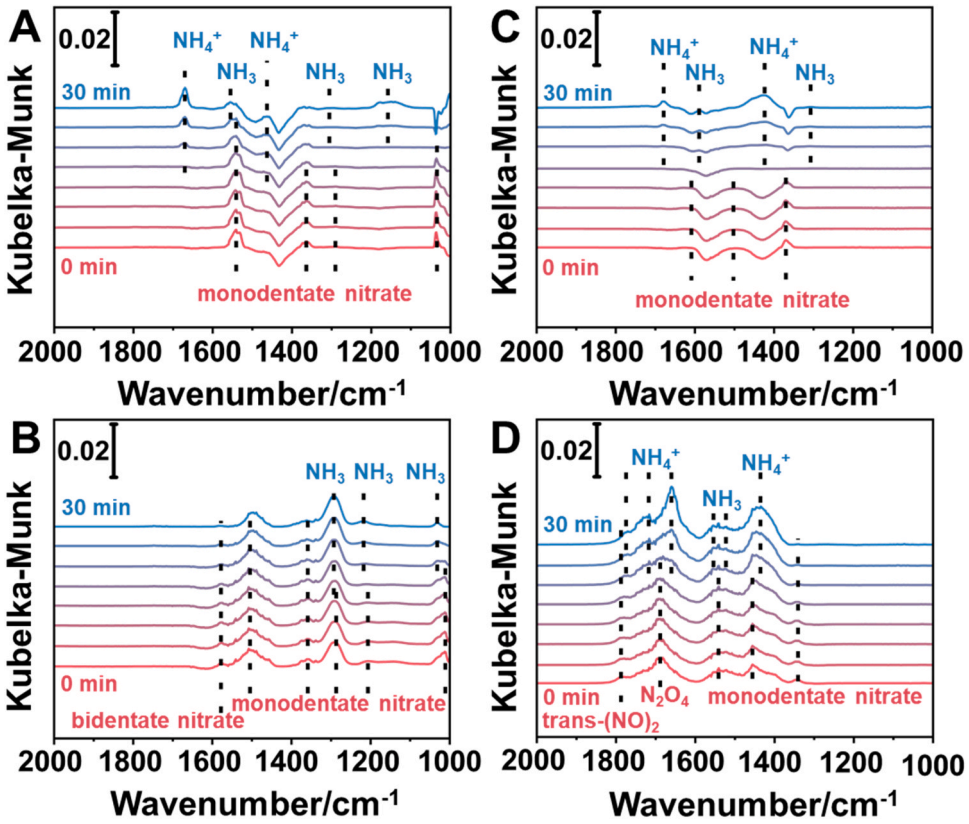

Fig. 9. *In situ* DRIFTS of the transient reaction upon passing NH_3 (1000 ppm) over (A) V/C, (B) K&Zn-V/C, (C) V/CSC, (D) K&Zn-V/CSC catalysts with NO (1000 ppm)+O_2 (5 vol% O_2/He) pre-adsorbed at 240 °C as a function of time.

facilitated. This demonstrated that introduction of $Ce(SO_4)_2$ additive not only certainly maintained the adsorption of NH_3 species and the generation of nitrates species, while also released the active V sites from poisoning to promote the activation and reaction between adsorbed NH_3 and nitrates species over the K&Zn-V/CSC catalyst due to the fact that $Ce(SO_4)_2$ was successfully utilized to be effectively combined with K and Zn poisons.

The self-tunable defense mechanism of the V/CSC catalyst against alkali metal K and heavy metal Zn co-poisoning was supposed in Fig. 10. On the fresh V/C catalyst, the NH_3/NH_4^+ species adsorbed on active sites could react with adsorbed NO_3^- species to generate N_2 and H_2O. With the introduction of $Ce(SO_4)_2$ additive, the adsorption capacity of NH_3 was slightly decreased and mainly due to active V=O species could provide more strong acid sites than $Ce(SO_4)_2$ additive. Meanwhile, the $Ce(SO_4)_2$ additive slightly restrained the electron transfer between V and Ce species and decrease the redox property of catalyst. However, the active vanadium species polymerization was enhanced and the acidity was enriched with the utilization of $Ce(SO_4)_2$ thus advantaging the reaction

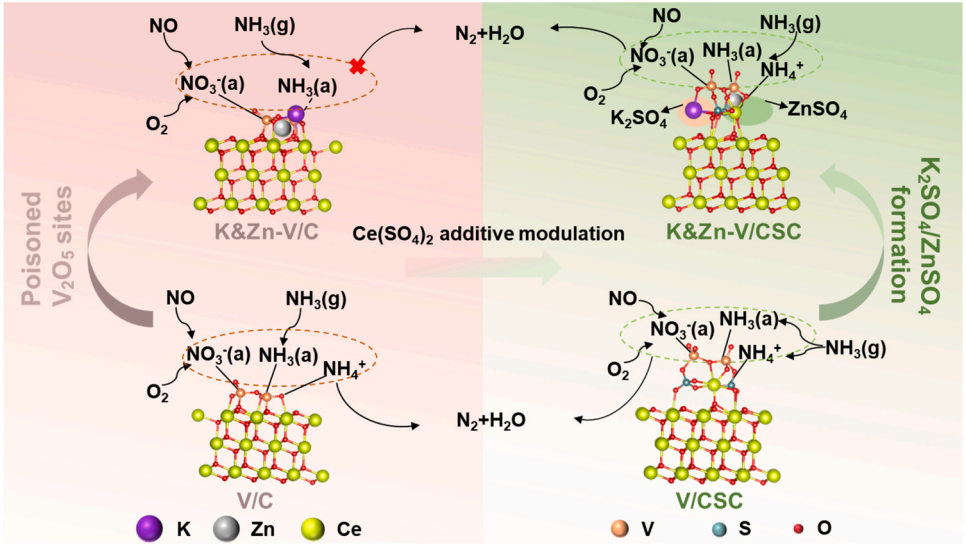

Fig. 10. Schematic illustration of defense mechanism of K and Zn co-poisoning over V/C and V/CSC catalysts for NO_x reduction (solid lines: strong adsorption, dash lines: weak adsorption).

to generate N_2 and H_2O over the V/CSC catalyst. After co-poisoning, due to the occupation of active sites by K and Zn poisons made active VO_x polymer translate to inactive monomers, the adsorption of active NH_3 and NO_x species were both severely inhibited and thus hindering the reaction of NO_x catalytic reduction over the K&Zn-V/C catalyst. In contrast, $Ce(SO_4)_2$ additive could surprisingly translate to a promoter to effectively combine with K and Zn poisons and also reduce the inhibiting effects of $Ce(SO_4)_2$ additive on the electron transfer between V and Ce over the K&Zn-V/CSC catalyst, thus ensuring the reaction of NO_x catalytic reduction was smoothly proceeded and maintaining the high catalytic activity of catalyst.

4. Conclusion

In summary, we thoroughly elucidated the self-tunable defense effect of $Ce(SO_4)_2$ additive modulation for the V_2O_5/CeO_2 catalyst with excellent resistance against alkali and heavy metals co-poisoning. The NO_x conversion of V/C and V/CSC catalysts demonstrated above 80% over a temperature range of 150–420 °C. After co-poisoning by K and Zn, the K&Zn-V/C catalyst displayed severe deactivation with below 10% of NO_x conversion remained. On the contrary, the K&Zn-V/CSC catalyst mostly retained its initial activity with over 80% of NO_x conversion from 240 to 420 °C. Although under humid conditions, the NO_x conversion and reaction rate of K&Zn-V/CSC were still significantly higher than that of K&Zn-V/C. It was characterized that the introduced facile and cheap $Ce(SO_4)_2$ additive would first act as an inhibitor to certainly restrain the electron transfer between V and Ce species to decrease the redox property, but superior NO_x reduction activity of the fresh catalyst could be maintained due to the enhancement of vanadium species polymerization and enrichment of acidity. More importantly, the $Ce(SO_4)_2$ additive could smartly translate to act as a promoter over the co-poisoned catalyst, which effectively combined with alkali and heavy metals poisons and released the inhibiting effect of electron transfer between V and Ce species, thus exhibiting the superior co-poisoning resistance over the $Ce(SO_4)_2$ additive modified V_2O_5/CeO_2 catalyst. The cheap and available $Ce(SO_4)_2$ additive modulation would help to promote most of metal oxides NH_3-SCR catalysts to save the cost of frequently replacing and regenerating, ensuring a wide prospect for alkali and heavy metal-resistant catalysts designing for the ultra-low emission of NO_x in waste incineration furnace, coal-fired power plant, biomass combustion furnaces, and other NO_x emission source contained high content of alkali and heavy metals.

CRediT authorship contribution statement

Heyang Hailun: Formal analysis, Data curation. **Lan Tianwei:** Formal analysis, Data curation. **Li Jin:** Investigation, Data curation. **Wang Lulu:** Writing – original draft, Investigation. **Zhang Dengsong:** Writing – review & editing, Validation, Supervision, Software, Resources, Project administration, Investigation, Funding acquisition, Conceptualization. **Wang Penglu:** Writing – review & editing, Validation, Investigation, Formal analysis, Data curation. **Wang Huan:** Formal analysis, Data curation.

Declaration of Competing Interest

All authors declare that there are no conflicts of interest, financial or otherwise in this work; and there are no other relationships or activities that can appear to have influenced the submitted work.

Data availability

Data will be made available on request.

Acknowledgments

We acknowledge the support of the National Key R&D Program of China (2023YFA1508400), National Natural Science Foundation of China (22276119; 22125604) and Chenguang Program supported by Shanghai Education Development Foundation and Shanghai Municipal Education Commission (21CGA48).

Appendix A. Supporting information

Supplementary data associated with this article can be found in the online version at doi:10.1016/j.apcatb.2024.123797.

References

[1] G. He, Z. Lian, Y. Yu, Y. Yang, K. Liu, X. Shi, Z. Yan, W. Shan, H. He, Polymeric vanadyl species determine the low-temperature activity of V-based catalysts for the SCR of NO_x with NH_3, Sci. Adv. 4 (2018) eaau4637.
[2] C. Paolucci, I. Khurana, A.A. Parekh, S. Li, A.J. Shih, H. Li, J.R.D. Iorio, J. D. Albarracin-Caballero, A. Yezerets, J.T. Miller, W.N. Delgass, F.H. Ribeiro, W. F. Schneider, R. Gounder, Dynamic multinuclear sites formed by mobilized copper ions in NO_x selective catalytic reduction, Science 357 (2017) 898–903.
[3] A. Richter, J.P. Burrows, H. Nüß, C. Granier, U. Niemeier, Increase in tropospheric nitrogen dioxide over China observed from space, Nature 437 (2005) 129–132.
[4] N.Y. Topsøe, Mechanism of the selective catalytic reduction of nitric oxide by ammonia elucidated by in situ on-line fourier transform infrared spectroscopy, Science 265 (1994) 1217–1219.
[5] Y. Peng, W. Si, J. Luo, W. Su, H. Chang, J. Li, J. Hao, J. Crittenden, Surface tuning of $La_{0.5}Sr_{0.5}CoO_3$ perovskite catalysts by acetic acid for NO_x storage and reduction, Environ. Sci. Technol. 50 (2016) 6442–6448.
[6] X. Hu, L. Huang, J. Zhang, H. Li, K. Zha, L. Shi, D. Zhang, Facile and template-free fabrication of mesoporous 3D nanosphere-like $Mn_xCo_{3-x}O_4$ as highly effective catalysts for low temperature SCR of NO_x with NH_3, J. Mol. Catal. A: Chem. 6 (2018) 2952–2963.
[7] R. Xie, L. Ma, Z. Li, Z. Qu, N. Yan, J. Li, Review of sulfur promotion effects on metal oxide catalysts for NO_x emission control, ACS Catal. 11 (2021) 13119–13139.
[8] X. Li, X. Li, T. Zhu, Y. Peng, J. Li, J. Hao, Extraordinary deactivation offset effect of arsenic and calcium on CeO_2-WO_3 SCR catalysts, Environ. Sci. Technol. 52 (2018) 8578–8587.
[9] L. Han, S. Cai, M. Gao, J.Y. Hasegawa, P. Wang, J. Zhang, L. Shi, D. Zhang, Selective catalytic reduction of NO_x with NH_3 by using novel catalysts: State of the art and future prospects, Chem. Rev. 119 (2019) 10916–10976.
[10] S. Jiang, Q. Su, Y. Yin, T. Zhu, X. Li, Extraordinary detoxification effect of arsenic on the cadmium-poisoned V_2O_5/TiO_2 catalyst for selective catalytic reduction of NO_x by NH_3, ACS Est. Eng. 3 (2023) 725–733.
[11] S. Cai, T. Xu, P. Wang, L. Han, S. Impeng, Y. Li, T. Yan, G. Chen, L. Shi, D. Zhang, Self-protected CeO_2-SnO_2@SO_4^{2-}/TiO_2 catalysts with extraordinary resistance to alkali and heavy metals for NO_x reduction, Environ. Sci. Technol. 54 (2020) 12752–12760.
[12] Z. Shen, X. Liu, S. Impeng, C. Zhang, T. Yan, P. Wang, D. Zhang, Alkali and heavy metal copoisoning resistant catalytic reduction of NO_x via liberating Lewis acid sites, Environ. Sci. Technol. 56 (2022) 5141–5149.
[13] Y. Pan, Z. Wu, J. Zhou, J. Zhao, X. Ruan, J. Liu, G. Qian, Chemical characteristics and risk assessment of typical municipal solid waste incineration (MSWI) fly ash in China, J. Hazard. Mater. 261 (2013) 269–276.
[14] B. Zhu, W. Chen, J. Wang, Y. Sun, W. Song, Z. Zi, H. Yu, E. Liu, Heavy metal poisoning resistance of a Co-modified 3Mn10Fe/Ni low-temperature SCR deNO_x catalyst, Environ. Sci. Pollut. Res. 28 (2020) 14546–14554.
[15] W. Li, R. Guo, S. Wang, W. Pan, Q. Chen, M. Li, P. Sun, S. Liu, The enhanced Zn resistance of Mn/TiO_2 catalyst for NH_3-SCR reaction by the modification with Nb, Fuel Process. Technol. 154 (2016) 235–242.
[16] S. Jiang, X. Li, Y. Yin, B. Luo, A.G. Isah, Z. Zhang, T. Zhu, Extraordinary deactivation offset effect of zinc and arsenic on V_2O_5-WO_3/TiO_2 catalysts: Like cures like, J. Hazard. Mater. 441 (2023) 129894.
[17] A.C. Larsson, J. Einvall, A. Andersson, M. Sanati, Targeting by comparison with laboratory experiments the SCR catalyst deactivation process by potassium and zinc salts in a large-scale biomass combustion boiler, Energy Fuels 20 (2006) 1398–1405.
[18] J. Cao, C. Nannuzzi, V. Lagostina, M.C. Paganini, W. Liu, H. Wu, Y. Gao, Q. Liu, G. Berlier, Insights into the poisoning mechanisms of zinc compounds on V_2O_5-WO_3/TiO_2 catalyst for NH_3-SCR: Effect of the anion species, J. Environ. Chem. Eng. 11 (2023) 109716.
[19] S. Li, H. Yu, T. Lan, L. Shi, D. Cheng, L. Han, D. Zhang, NO_x reduction against alkali poisoning over $Ce(SO_4)_2$-V_2O_5/TiO_2 catalysts by constructing the Ce^{4+}–SO_4^{2-} pair sites, Chin. Chem. Lett. (2023) 108240.
[20] J.A. Poston, R.V. Siriwardane, E.P. Fisher, A.L. Miltz, Thermal decomposition of the rare earth sulfates of cerium(III), cerium(IV), lanthanum(III) and samarium (III), Appl. Surf. Sci. 214 (2003) 83–102.
[21] Y. Peng, C. Wang, J. Li, Structure–activity relationship of VO_x/CeO_2 nanorod for NO removal with ammonia, Appl. Catal. B: Environ. 144 (2014) 538–546.

[22] Y. Peng, J. Li, X. Huang, X. Li, W. Su, X. Sun, D. Wang, J. Hao, Deactivation mechanism of potassium on the V_2O_5/CeO_2 catalysts for SCR reaction: acidity, reducibility and adsorbed-NO_x, Environ. Sci. Technol. 48 (2014) 4515–4520.
[23] X. Gao, I. Wachs, Investigation of surface structures of supported vanadium oxide catalysts by UV–vis-NIR diffuse reflectance spectroscopy, J. Phys. Chem. B. 104 (2000) 1261–1268.
[24] P. Zhang, P. Wang, A. Chen, L. Han, T. Yan, J. Zhang, D. Zhang, Alkali-resistant catalytic reduction of NO_x by using Ce-O-B alkali-capture sites, Environ. Sci. Technol. 55 (2021) 11970–11978.
[25] M.N. Khan, L. Han, P. Wang, D. Zhang, Tailored alkali resistance of deNO_x catalysts by improving redox properties and activating adsorbed reactive species, iScience 23 (2020).
[26] X. Liu, K. Zhou, L. Wang, B. Wang, Y. Li, Oxygen vacancy clusters promoting reducibility and activity of ceria nanorods, J. Am. Chem. Soc. 131 (2009) 3140–3141.
[27] H. Wang, Z. Qu, H. Xie, N. Maeda, L. Miao, Z. Wang, Insight into the mesoporous $Fe_xCe_{1-x}O_{2-\delta}$ catalysts for selective catalytic reduction of NO with NH_3: Regulable structure and activity, J. Catal. 338 (2016) 56–67.
[28] Y. Zhao, L. Shi, Y. Shen, J. Zhou, Z. Jia, T. Yan, P. Wang, D. Zhang, Self-defense effects of Ti-modified attapulgite for alkali-resistant NO_x catalytic reduction, Environ. Sci. Technol. 56 (2022) 4386–4395.
[29] G. Zhou, P. Maitarad, P. Wang, L. Han, T. Yan, H. Li, J. Zhang, L. Shi, D. Zhang, Alkali-resistant NO_x reduction over SCR catalysts via boosting NH_3 adsorption rates by in situ constructing the sacrificed sites, Environ. Sci. Technol. 54 (2020) 13314–13321.
[30] G. Went, L. Leu, A. Bell, Quantitative structural analysis of dispersed vanadia species in TiO_2(anatase)-supported V_2O_5, J. Catal. 134 (1992) 479–491.
[31] M. Lyu, J. Zou, X. Liu, T. Yan, P. Wang, D. Zhang, Insight on the anti-poisoning mechanism of in situ coupled sulfate over iron oxide catalysts in NO_x reduction, Catal. Sci. Technol. 12 (2022) 4020–4031.
[32] J. Zhang, Z. Huang, Y. Du, X. Wu, H. Shen, G. Jing, Alkali-poisoning-resistant $Fe_2O_3/MoO_3/TiO_2$ catalyst for the selective reduction of NO by NH_3: The role of the MoO_3 safety buffer in protecting surface active sites, Environ. Sci. Technol. 54 (2020) 595–603.
[33] Z. Hao, Z. Shen, Y. Li, H. Wang, L. Zheng, R. Wang, G. Liu, S. Zhan, The role of alkali metal in alpha-MnO_2 catalyzed ammonia-selective catalysis, Angew. Chem., Int. Ed. 58 (2019) 6351–6356.
[34] X. Wang, Q. Cong, L. Chen, Y. Shi, Y. Shi, S. Li, W. Li, The alkali resistance of CuNbTi catalyst for selective reduction of NO by NH_3: A comparative investigation with VWTi catalyst, Appl. Catal. B: Environ. 246 (2019) 166–179.
[35] Y. Yu, J. Wang, J. Chen, X. Meng, Y. Chen, C. He, Promotive effect of SO_2 on the activity of a deactivated commercial selective catalytic reduction catalyst: An in situ DRIFT study, Ind. Eng. Chem. Res. 53 (2014) 16229–16234.
[36] J. Wang, Z. Yan, L. Liu, Y. Chen, Z. Zhang, X. Wang, In situ DRIFTS investigation on the SCR of NO with NH_3 over V_2O_5 catalyst supported by activated semi-coke, Appl. Surf. Sci. 313 (2014) 660–669.
[37] Y. Zhang, X. Yue, T. Huang, K. Shen, B. Lu, In situ DRIFTS studies of NH_3-SCR mechanism over V_2O_5-CeO_2/TiO_2-ZrO_2 catalysts for selective catalytic reduction of NO_x, Materials 11 (2018) 1307.
[38] X. Weng, X. Dai, Q. Zeng, Y. Liu, Z. Wu, DRIFT studies on promotion mechanism of $H_3PW_{12}O_{40}$ in selective catalytic reduction of NO with NH_3, J. Colloid Interface Sci. 461 (2016) 9–14.
[39] L. Chen, Z. Si, X. Wu, D. Weng, DRIFT study of CuO-CeO_2-TiO_2 mixed oxides for NO_x reduction with NH_3 at low temperatures, ACS Appl. Mater. 6 (2014) 8134–8145.
[40] H. Hu, S. Cai, H. Li, L. Huang, L. Shi, D. Zhang, In situ DRIFTs investigation of the low-temperature reaction mechanism over Mn-Doped Co_3O_4 for the selective catalytic reduction of NO_x with NH_3, J. Phys. Chem. C. 119 (2015) 22924–22933.
[41] R. Wu, N. Zhang, L. Li, H. He, L. Song, W. Qiu, DRIFT study on promotion effect of the keggin structure over V_2O_5-MoO_3/TiO_2 catalysts for low temperature NH_3-SCR reaction, Catalysts 8 (2018).
[42] L. Huang, K. Zha, S. Namuangruk, A. Junkaew, X. Zhao, H. Li, L. Shi, D. Zhang, Promotional effect of the TiO_2 (001) facet in the selective catalytic reduction of NO with NH_3: in situ DRIFTS and DFT studies, Catal. Sci. Technol. 6 (2016) 8516–8524.
[43] H. Hu, S. Cai, H. Li, L. Huang, L. Shi, D. Zhang, Mechanistic aspects of deNO_x processing over TiO_2 supported Co–Mn oxide catalysts: structure–activity relationships and in situ DRIFTs analysis, ACS Catal. 5 (2015) 6069–6077.
[44] K. Zha, S. Cai, H. Hu, H. Li, T. Yan, L. Shi, D. Zhang, In situ DRIFTs investigation of promotional effects of tungsten on MnO_x-CeO_2/meso-TiO_2 catalysts for NO_x reduction, J. Phys. Chem. C. 121 (2017) 25243–25254.
[45] Q. Zhang, J. Fan, P. Ning, Z. Song, X. Liu, L. Wang, J. Wang, H. Wang, K. Long, In situ DRIFTS investigation of NH_3-SCR reaction over CeO_2/zirconium phosphate catalyst, Appl. Surf. Sci. 435 (2018) 1037–1045.
[46] Z. Zhang, L. Chen, Z. Li, P. Li, F. Yuan, X. Niu, Y. Zhu, Activity and SO_2 resistance of amorphous CeaTiOx catalysts for the selective catalytic reduction of NO with NH_3: in situ DRIFT studies, Catal. Sci. Technol. 6 (2016) 7151–7162.
[47] L. Ma, Y. Cheng, G. Cavataio, R.W. McCabe, L. Fu, J. Li, In situ DRIFTS and temperature-programmed technology study on NH_3-SCR of NO over Cu-SSZ-13 and Cu-SAPO-34 catalysts, Appl. Catal. B: Environ. 156-157 (2014) 428–437.
[48] Z. Liu, S. Zhang, J. Li, L. Ma, Promoting effect of MoO_3 on the NO_x reduction by NH_3 over CeO_2/TiO_2 catalyst studied with in situ DRIFTS, Appl. Catal. B: Environ. 144 (2014) 90–95.
[49] D. Wang, J. Luo, Q. Yang, J. Yan, K. Zhang, W. Zhang, Y. Peng, J. Li, J. Crittenden, Deactivation mechanism of multipoisons in cement furnace flue gas on selective catalytic reduction catalysts, Environ. Sci. Technol. 53 (2019) 6937–6944.
[50] K. Liu, F. Liu, L. Xie, W. Shan, H. He, DRIFTS study of a Ce–W mixed oxide catalyst for the selective catalytic reduction of NO_x with NH_3, Catal. Sci. Technol. 5 (2015) 2290–2299.
[51] J. Liu, X. Li, Q. Zhao, J. Ke, H. Xiao, X. Lv, S. Liu, M. Tadé, S. Wang, Mechanistic investigation of the enhanced NH_3-SCR on cobalt-decorated Ce-Ti mixed oxide: In situ FTIR analysis for structure-activity correlation, Appl. Catal., B. 200 (2017) 297–308.
[52] W. Tan, C. Wang, S. Yu, Y. Li, S. Xie, F. Gao, L. Dong, F. Liu, Revealing the effect of paired redox-acid sites on metal oxide catalysts for efficient NO_x removal by NH_3-SCR, J. Hazard. Mater. 416 (2021) 125826.
[53] L. Cao, L. Chen, X. Wu, R. Ran, T. Xu, Z. Chen, D. Weng, TRA and DRIFTS studies of the fast SCR reaction over CeO_2/TiO_2 catalyst at low temperatures, Appl. Catal., A. 557 (2018) 46–54.
[54] Z. Liu, H. Liu, X. Feng, L. Ma, X. Cao, B. Wang, Ni-Ce-Ti as a superior catalyst for the selective catalytic reduction of NO_x with NH_3, Mater. Charact. 445 (2018) 179–186.
[55] L. Chen, J. Li, M. Ge, DRIFT Study on Cerium−Tungsten-Titiania Catalyst for Selective Catalytic Reduction of NO_x with NH_3, Environ. Sci. Technol. 44 (2010) 9590–9596.
[56] P. Zhang, P. Wang, S. Impeng, T. Lan, X. Liu, D. Zhang, Unique compensation effects of heavy metals and phosphorus copoisoning over NO_x reduction catalysts, Environ. Sci. Technol. 56 (2022) 12553–12562.
[57] J. Liu, J. Meeprasert, S. Namuangruk, K. Zha, H. Li, L. Huang, P. Maitarad, L. Shi, D. Zhang, Facet–activity relationship of TiO_2 in Fe_2O_3/TiO_2 nanocatalysts for selective catalytic reduction of NO with NH_3: In situ DRIFTs and DFT studies, J. Phys. Chem. C. 121 (2017) 4970–4979.
[58] P. Zhang, A. Chen, T. Lan, X. Liu, T. Yan, W. Ren, D. Zhang, Balancing acid and redox sites of phosphorylated CeO_2 catalysts for NO_x reduction: The promoting and inhibiting mechanism of phosphorus, J. Hazard. Mater. 441 (2023) 129867.